

Ⓞ The Intracloud Lightning Fraction in the Contiguous United States

GINA MEDICI AND KENNETH L. CUMMINS^a

Department of Hydrology and Atmospheric Sciences, The University of Arizona, Tucson, Arizona

DANIEL J. CECIL AND WILLIAM J. KOSHAK

NASA George C. Marshall Space Flight Center/NSSTC, Huntsville, Alabama

SCOTT D. RUDLOSKY

NOAA/NESDIS/STAR, College Park, Maryland


(Manuscript received 14 November 2016, in final form 1 July 2017)


ABSTRACT

This work addresses the long-term relative occurrence of cloud-to-ground (CG) and intracloud (IC; no attachment to ground) flashes for the contiguous United States (CONUS). It expands upon an earlier analysis by Boccippio et al. who employed 4-yr datasets provided by the U.S. National Lightning Detection Network (NLDN) and the Optical Transient Detector (OTD). Today, the duration of the NLDN historical dataset has more than tripled, and OTD data can be supplemented with data from the Lightning Imaging Sensor (LIS). This work is timely, given the launch of *GOES-16*, which includes the world's first geostationary lightning mapper that will observe total lightning (IC and CG) over the Americas and adjacent ocean regions. Findings support earlier results indicating factor-of-10 variations in the IC:CG ratio throughout CONUS, with climatological IC fraction varying between 0.3 and greater than 0.9. The largest values are seen in the Pacific Northwest, central California, and where Colorado borders Kansas and Nebraska. An uncertainty analysis indicates that the large values in the northwest and central California are likely not due to measurement uncertainty. The high IC:CG ratio (>4) throughout much of Texas reported by Boccippio et al. is not supported by this longer-term climatology. There is no clear evidence of differences in IC fraction between land and coastal ocean. Lightning characteristics in six selected large regions show a consistent positive relationship between IC fraction and the percent of positive CG flashes, irrespective of lightning incidence (flash density), dominant season, or diurnal maximum period.

1. Introduction

For decades, lightning research has contributed not only to our understanding of the basic lightning processes and physics, but to a better understanding of the

 Denotes content that is immediately available upon publication as open access.

 Supplemental information related to this paper is available at the Journals Online website: <https://doi.org/10.1175/MWR-D-16-0426.s1>.

^a ORCID: 0000-0001-9871-691X.

Corresponding author: Kenneth L. Cummins, kcummins@email.arizona.edu

weather and climatology of deep convection. Advances in lightning detection and geolocation (summarized in [Cummins and Murphy 2009](#); [Nag et al. 2015](#); [Ushio et al. 2015](#)) have made essential contributions to our increasing knowledge in these areas. In addition, satellite observations of the diffuse cloud-top optical emissions produced from lightning since 1995 provide global climatologies of total lightning [(TL); all lightning flashes, including those that produce channels to ground] ([Christian et al. 2003](#); [Mach et al. 2007](#); [Cecil et al. 2014](#), hereafter [C14](#); [Cecil et al. 2015](#)). When coupled with climatological incidence of cloud-to-ground (CG) flashes, these data provided our first spatially contiguous view of the relative occurrence of intracloud (IC) flashes and CG flashes ([Boccippio et al. 2001](#), hereafter [B01](#)). This work depicted the relative occurrence of IC and CG flashes by the IC:CG ratio, which was first defined by [Mackerras \(1985\)](#) as the *Z* ratio. Some later

DOI: 10.1175/MWR-D-16-0426.1

© 2017 American Meteorological Society. For information regarding reuse of this content and general copyright information, consult the [AMS Copyright Policy](#) (www.ametsoc.org/PUBSReuseLicenses).

publications have recommended the use of either the “cloud flash (or IC) fraction” (fraction of flashes that do not attach to the ground) or “ground (or CG) fraction” (fraction of flashes with one or more ground attachments). Both alternative depictions avoid the numerical singularity in IC:CG ratio when the CG fraction is zero, as well as numerical instabilities (i.e., excessive sensitivity) in IC:CG ratio to small changes in the CG fraction when it is near zero. The work presented here addresses this issue in more detail, and we employ the terminology IC:CG ratio, IC fraction, and CG fraction.

The orbital nature of the satellite TL observations to date (few minutes of continuous observation at any one location for any one overpass) makes it impossible for these data to be used to assess the time evolution of individual storms. However, a significant next step in lightning detection is the recent launch of the first Geostationary Lightning Mapper (GLM) on board the Geostationary Operational Environment Satellite R (GOES-R) series. The GOES-R satellite reached geostationary orbit on 29 November 2016 and is now called *GOES-16*. After an approximately 9-month Post Launch Test and validation phase, GLM will provide fully validated continuous TL observations with near-uniform spatial resolution by measuring radiance at the cloud tops produced by all types of lightning [see [Goodman et al. \(2013\)](#) for additional benefits of GLM]. The *GOES-16* will replace GOES-East and GOES-S/17 will replace GOES-West as shown in Fig. 2 of [Goodman et al. \(2013\)](#). Because GLM will capture the entire spatiotemporal evolution of storms within its wide field of view, it is expected to improve our ability to extend severe weather warning times [[Schultz et al. \(2011, 2015\)](#) and references therein], and will provide valuable data for short-term forecasting of convective precipitation and severe weather outbreaks ([Fierro et al. 2015, 2016](#)). More broadly, GLM will provide critical data that will contribute to our understanding of differences in thunderstorm behavior over land and ocean, and as a function of time of day and season.

There are physical reasons why a storm preferentially produces IC or CG lightning. A typical (simplified) electrified cloud is explained as having vertical layers of electrical charge composed of an upper positive charge below the tropopause, a midlevel negative charge region well above the freezing level, and a much smaller positive charge layer below it ([Williams 1989](#)). Intracloud flashes generally “neutralize” charge between the upper positive and midlevel negative charge regions in a cloud while CG flashes typically transfer negative charge to one or more locations on the ground. The relative occurrence of IC and CG flashes is thought to be determined in part by the relative locations and sizes of these charge centers, and

their spatial relationship to the terrain below. Additionally, the existence and nature of the lower positive charge center has a significant influence on the occurrence of CG flashes ([Jacobson and Krider 1976](#)). When there is a large positive charge center at low altitude above ground level, this can also inhibit the production of negative CG flashes ([Nag and Rakov 2009](#); [Mansell et al. 2010](#)). Storms that exhibit inverted and/or complex charge structures frequently have high IC flash rates, discourage the production of negative CG flashes, and encourage the production of positive CG flashes within the convective region of the storm ([Carey and Rutledge 1998, 2003](#); [Wiens et al. 2005](#); [Carey and Buffalo 2007](#); [Qie et al. 2009](#); [Bruning et al. 2014](#); [Fuchs et al. 2015](#)). Sections 7.20 and 7.21 in [MacGorman and Rust \(1998\)](#) provide additional details. Helpful modeling work on this topic is presented in [Mansell et al. \(2010\)](#).

There is value in refining our understanding of the long-term regional differences in the occurrence of IC and CG flashes, for several reasons. Most urgently, the upcoming real-time use of GLM TL data by forecasters in the Americas makes it imperative that they have a clear understanding of the “nominal” regional differences in the occurrence of IC and CG flashes, as they become familiar with the GLM dataset and interrelate it with the existing CG and TL datasets provided by ground-based LLS networks. This is important because of a three- to tenfold regional climatological variation in the fraction of flashes that attach to ground ([Mackerras et al. 1998](#); [B01](#); [Pinto et al. 2003](#); [Soriano and de Pablo 2007](#); and the references therein). An understanding of these regional variations will help forecasters understand and properly interpret the short-term changes in TL and CG flash rates when evaluating individual storms that move into and out of different climate regimes.

Beyond the operational needs, there are several uses of lightning data that require knowledge of the relative occurrence of IC and CG flashes, some of which are briefly described here. An important practical issue is the interpretation of comparisons between satellite-derived lightning datasets and ground-based LLS datasets that preferentially report return strokes in CG flashes, such as the work by [Thompson et al. \(2014\)](#) and [Rudlosky and Shea \(2013\)](#). For these uses, the observed proportion of time- and space-coincident lightning reports are weighted by both the relative occurrence of IC and CG flashes and by the LLS’s different detection efficiencies for these types of flashes. More broadly, the analysis of the climatological behavior of any atmospheric electrical, chemical, or precipitation-related parameter that has a fundamental relationship with flash type requires knowledge of the relative occurrence of IC and CG flashes ([Beirle et al. 2014](#)). Important

examples include estimation of lightning NO_x production (Beirle et al. 2010; Koshak et al. 2014; Ott et al. 2010), and assessment of the electrical current contributed to the global circuit by individual storms (Driscoll et al. 1992, 1994; Mareev et al. 2008).

Temporal variations in the occurrence of IC and CG flashes at short time scales will influence their relative occurrence at the climatological time scale. The simplest possible explanation for the more frequent occurrence of IC flashes would be that the IC flash rate per unit area is higher whenever there is lightning, and that IC flashes occur in the same proportion over short and long time periods. However, this is not the case. Considering short time scales, the life cycle of typical thunderstorms can be broken down into initial, active, and final phases. For Florida thunderstorms, Livingston and Krider (1978) found that very few CG flashes occurred during the initial phase, about half of the flashes during the active phase were CG, and 20% of the flashes during the final phase were CG. Krehbiel (1986) indicates that the delayed occurrence of CG flashes is in concert with increasing height of the upper positive charge region during storm development, relative to the nearly stable height of the main negative charge region. Jacobson and Krider (1976) noted that development of the lower positive charge region, which naturally evolves during the development of a storm, is influenced by the occurrence of lightning flashes.

The details related to this overall sequence vary by region and storm type. MacGorman et al. (2011) report large regional variability in the latency of the first CG flash in thunderstorms in the central United States, and showed that the largest average latency was in the high plains where the climatological proportion of flashes striking the ground is quite small. This region also exhibits the largest percentage of positive polarity CG flashes. Additionally, storm severity is frequently associated with strong updrafts producing large mass flux through the mixed phase region, which is conducive to smaller flash sizes, higher IC flash rates, and sometimes associated with a reduction or elimination of CG flashes (MacGorman et al. 1989; Williams et al. 1999; Wiens et al. 2005; MacGorman et al. 2011; Makowski et al. 2013; Bruning and MacGorman 2013; Fuchs et al. 2015). These findings suggest that as a storm “becomes severe,” it becomes more likely to exhibit a high flash rate [e.g., “lightning jump”—see Gatlin and Goodman (2010)] with most flashes being IC, also resulting in large temporal modulation of the relative occurrence of IC and CG flashes throughout the storm life cycle.

Given the broad value of understanding long-term regional variations in the relative occurrence of IC and CG flashes, we expand upon the earlier analysis by

reference B01 using additional and longer-term datasets. We note that any long-term climate variations that change the characteristics of thunderstorms will likely have an associated impact on the types and characteristics of lightning produced. Hence, this work represents an important baseline measurement for, and contribution to, the ongoing National Climate Assessment (NCA) lightning-climate study first reported in Koshak et al. (2015).

The work presented here also includes a detailed quantitative assessment of uncertainties in the satellite-derived average annualized flash density (flashes km⁻²yr⁻¹), referred to in C14 as flash rate and in Holle (2014) (and in this work) as flash density. The uncertainties arise from the limited time sampling of thunderstorms because of the orbital nature of the satellites (to be discussed here in detail). The additional years of data beyond what was available to B01 also allows us to employ less spatial smoothing than was practical in B01, and to separate data sampling limitations from multi-year regional variability. Section 2 describes the datasets and analysis methods. Results and discussion are presented in section 3, followed by conclusions and future work (section 4).

2. Data and methods

This study uses the U.S. National Lightning Detection Network (NLDN) to provide the CG flash density climatology, and the Optical Transient Detector (OTD), the Lightning Imaging Sensor (LIS), and a combination of OTD and LIS (OTD/LIS) to provide the TL flash density climatology. Sections 2a–c briefly discuss these datasets and the methods used to evaluate and compare them.

We note that recent work by Koshak and Solakiewicz (2015) has demonstrated the possibility to infer the ground flash fraction directly from a detailed analysis of the satellite-derived lightning dataset, with an expected accuracy of about 80%. However, in our work, we employ the NLDN data because 1) its type classification accuracy is thought to be better (Nag et al. 2015), 2) it does not suffer from the sampling limitations of the OTD/LIS datasets described later, and 3) the results can be directly compared to the climatology produced by B01.

a. NLDN data

The NLDN has been providing lightning data since the early 1980s, and since 1989 has been used for continental-scale lightning research in the United States (Cummins and Murphy 2009). The NLDN was originally composed of gated wide-band magnetic direction finders that employed magnetic field waveforms to determine the direction to the channel bases of lightning

TABLE 1. Summary of data used in this study.

Data	Lightning type	Years	Domain	Flash DE
OTD	Total	May 1995–Mar 2000	$\pm 75^\circ$ lat	0.37–0.51 (varies with time of day, location, and sensor threshold settings)
LIS	Total	1998–2013	$\pm 38^\circ$ lat	0.69–0.88 (varies with time of day)
OTD/LIS	Total	May 1995–31 Dec 2013	$\pm 75^\circ$ lat	DE corrections applied (C14, Fig. 2)
NLDN	CG	May 1995–31 Dec 2013	CONUS	0.7–0.95 (varies by location and year; see appendix B)

discharge to the ground (Krider et al. 1976). The first major improvement to the NLDN occurred in 1995 when the direction finders were upgraded to include GPS timing data, resulting in the so-called Improved Accuracy through Combined Technology (IMPACT) sensor (Cummins et al. 1998). The IMPACT geolocation algorithm computes the latitude, longitude, and discharge time using as few as two sensors (Cummins and Murphy 2009). The CG flash detection efficiency (DE) following this upgrade ranged between 70% and 90% over much of the interior of the network, and was below 60% at or near the edges of the network (Cummins et al. 1998). In 2002–03, the NLDN improved when all NLDN sensors were replaced with better IMPACT-ESP sensors and eight additional sensors were added to the network. This further improved the flash DE to between 90% and 95% (Cummins and Murphy 2009) among other changes (Rudlosky and Fuelberg 2010). The spatial boundaries of the NLDN are 250 km into Canada, 600 km into Mexico, and 600 km into the Pacific and Atlantic Oceans (Holle 2014). The flash DE decreases in all directions outside the contiguous United States (CONUS) except Canada, where the Canadian Lightning Detection Network (CLDN) has been used in conjunction with the NLDN since 1998 (Orville et al. 2011). As a result of a 2013 upgrade to the NLDN, the estimated CG flash DE improved from about 90% for the period of 2003–12 to over 95% throughout CONUS [see Nag et al. (2014) for details]. Somewhat variable performance over earlier years is addressed in this work by employing corrections for detection efficiency, as described in the online supplemental material. Prior to 1996, the NLDN did not report any discharges classified as cloud lightning. The number of reported IC flashes has steadily increased since that time. In the present study, only NLDN-reported CG flashes are employed. All small positive discharges (<15 kA) are excluded, as recommended by Cummins and Murphy (2009), to help minimize misclassification of IC and CG discharges. Some misclassification errors remain, and are discussed later in the context of their impact on findings in this work. A history of the recent NLDN upgrades, including performance implications, is provided in Koshak et al. (2015).

b. OTD and LIS

The OTD instrument provided TL data for 5 years (1995–2000) on the *OrbView-1* (*OV-1*) (formerly *MicroLab-1*) satellite (Mach et al. 2007; Christian et al. 2003), and recorded lightning between 75°N and 75°S (Christian et al. 2003). The flash DE has been reported to be between 49% and 65% (Boccippio et al. 2000; B01). OTD's field of view was about $1300 \times 1300 \text{ km}^2$ with a spatial resolution of 10 km and about 14 orbits each day (C14).

The LIS instrument was part of the Tropical Rainfall Measuring Mission that launched in 1997 and collected TL lightning observations until April 2015. The LIS orbit was limited to 38°N to 38°S with a flash DE of about 69% during local noon and 88% at night (C14). LIS's field of view changed from about $600 \times 600 \text{ km}^2$ to about $700 \times 700 \text{ km}^2$ following a boost in the TRMM satellite average altitude from $\sim 350 \text{ km}$ before August 2001 to $\sim 400 \text{ km}$ after August 2001. The respective spatial resolution changed from ~ 5 to $\sim 6 \text{ km}$. LIS had about 16 orbits each day (C14).

This analysis uses the global gridded OTD and LIS datasets produced by NASA (see C14 for a detailed description). More specifically, for the long-term climatology we employ the gridded flash rate product (flash density in units of $\text{flashes km}^{-2} \text{ yr}^{-1}$), which is part of the High Resolution Full Climatology (HRFC) dataset with a spatial resolution of $0.5^\circ \times 0.5^\circ$. The measured flash counts were scaled to correct for observation times and flash detection efficiency, as described in C14. Other OTD and LIS datasets are used for bias analyses, as described in appendix A.

This study examines the OTD and LIS data for the period of May 1995–December 2013. The combined OTD/LIS data provide the TL portion while NLDN is used for CG flashes, making it possible to determine the IC:CG ratio in the same manner as B01 who utilized four years of OTD and NLDN data. The result is an 18.5-yr flash density climatology equatorward of 38°N and a 5-yr climatology poleward of 38°N . Table 1 summarizes these datasets.

As noted earlier, the orbital nature of the OTD and LIS observations result in very limited observations

(sampling, or view time) for any specific location on the earth. The yearly OTD view time is between 12 and 16 h, accumulated from numerous individual overpasses lasting about 3 min (Christian et al. 2003). The LIS annual view time over CONUS is between 16 and 33 h, accumulated from numerous individual overpasses lasting about 90 s (C14). This limited sampling can result in seasonal and diurnal (time of day) biases in observation time, as compared to what would be observed with continuous observations. The HRFC and its low-resolution counterpart (LRDC) flash density datasets do not compensate for these differences in the view time as a function of season or time of day. Appendix A in this paper provides separate analyses of these biases for our analysis domain, analyzed separately for OTD (above 38°N) and LIS (below 38°N). These sources of error are much smaller than the estimated fractional RMS error due simply to limited overall view time (also covered in appendix A), which is in the range of 11%–23%. These findings led us to accept the HRFC climatologies, allowing us to employ the higher-resolution (0.5°) grids.

For most of the analyses presented here, the data were smoothed based on Gaussian smoothing with a standard deviation of one grid cell (0.5° resolution) using a 5×5 array of grid points. All smoothing was performed prior to any arithmetic manipulations (ratios, differences, etc.). This improves numerical stability since the datasets are small due to the limited view time. Assuming independent observation errors in the 24 neighboring grids used in smoothing, the RMS error in a grid estimate is reduced by a factor of 0.287. This smoothing approach allows somewhat more localized variation than the 3.5° “boxcar” smoothing (equal weighting for all related grid points) used by B01, which is justified by the additional periods of observation and the error analysis provided in appendix A. The color scales used in most maps were designed to avoid perceptual bias and to limit problems for readers with color-deficient vision (Stauffer et al. 2015). Contour lines were also added to most map-based figures to assist in identifying subtle color transitions.

In this work, we also compare the OTD and LIS datasets below 38°N to evaluate instrumentation or calibration biases in the datasets, and to set expectations for the variability in the 5-yr OTD climatology in the northern latitudes. The comparisons are carried out in two different ways: one is a signed (+/–) “spatial difference” map expressed as a percentage (like a “normalized anomaly” used in climatological studies), and the other is a histogram of the magnitude of this difference. The spatial difference shows locations where there is a strong bias toward one dataset, using the following equation:

$$\frac{100 \times (\text{OTD} - \text{LIS})}{(\text{OTD} + \text{LIS})/2}, \quad (1)$$

where OTD and LIS (used as variable in this equation) represent the flash density values for any given grid location.

Given the two-domain nature of the satellite-derived lightning density, an NLDN “composite” CG flash density dataset was constructed to match the time periods of the satellite-derived datasets. For this composite dataset, the NLDN data above 38°N was limited to the early 5-yr period, and the NLDN data below 38°N included all 18.5 years of data (see section 3b).

c. Lightning-type ratios

There are several possible ways to express the relative occurrence of IC and CG flashes. B01 employed the IC:CG ratio Z based on the body of prior literature. In this section, we provide a rationale for using the IC fraction as suggested by MacGorman and Rust (1998, their section 7.15). We note that the “CG fraction” (the fraction of all flashes with one or more ground attachments) is an equally appropriate and numerically well-behaved representation, but we hesitate to promote this parameter since it frequently approaches zero when there is severe weather.

In the equations provided below, we have employed variable names that are tied to the actual quantities to simplify interpretation of the equations, but these variables are only used here for mathematical definition and for development of sensitivity equations in appendix B. A “composite” IC:CG ratio (defined here as the variable R to improve readability) was calculated using the combined OTD/LIS dataset and the composite NLDN data as described above. The ratio R is calculated for each grid point using

$$R = \frac{C}{G} = \frac{T - G}{G}, \quad (2)$$

where T is the composite total lightning (OTD and LIS) flash density, G is the composite NLDN CG flash density, and C is the (computable) density of cloud flashes (those without ground attachments). The method used to estimate C in Eq. (2) has an influence on the uncertainty of the results. In this work, we simply subtract the ground flash density from the total lightning density to produce the cloud flash density. This implicitly assumes that OTD and LIS identify flashes with equivalent space–time properties as the CG flashes identified by the NLDN. However, it is reasonable to expect that the large cloud-top illumination areas associated with a single LIS or OTD flash will at times be associated with multiple distinct and spatially separated CG flashes; this

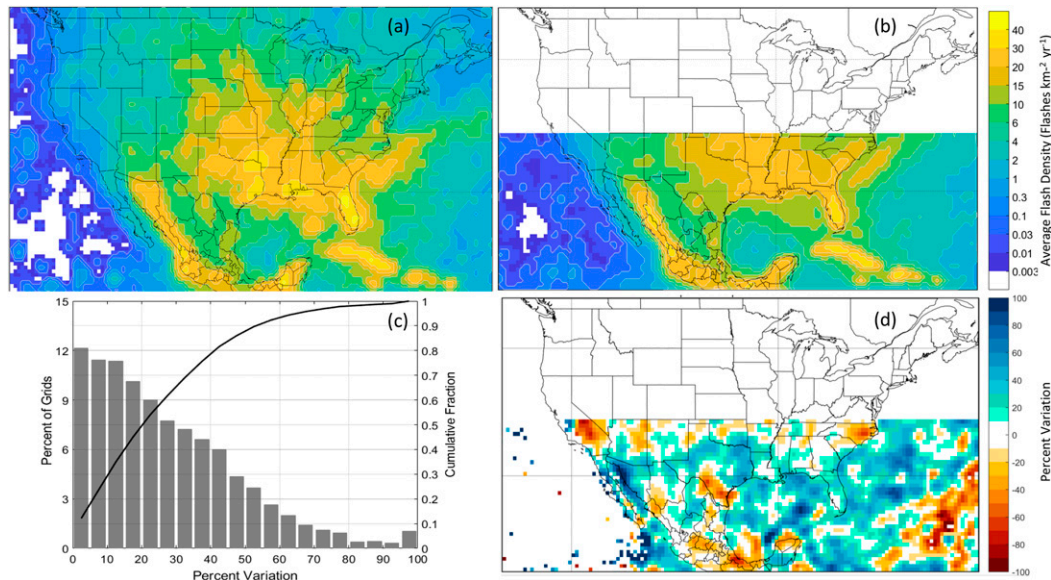


FIG. 1. Variability of satellite-derived total lightning flash density: (a) OTD data from 1995–99, (b) LIS data from 1998 to 2013, (c) OTD – LIS spatial difference magnitude (% deviation from mean) histogram and cumulative distribution, and (d) OTD – LIS spatial difference map. Negative values indicate higher density for LIS. Contour lines in (a) and (b) are placed at all color boundaries above $0.01 \text{ flashes km}^{-2} \text{ yr}^{-1}$.

was explicitly noted by Franklin (2013). Zhang et al. (2016) observed a 13.4% higher flash count reported by the NLDN for 507 carefully matched LIS flashes in 2013, but this is a rather limited dataset. This issue is discussed again in the interpretation of our findings.

When the CG flash density is small, the calculated value of the IC:CG ratio R will be sensitive to small variations in G . The IC fraction (F_c in these equations) does not suffer from this instability as much as R , and is given by the following equation:

$$F_c = \frac{T - G}{T}. \quad (3)$$

The technical appendix in B01 provides a detailed treatment of the impact of various measurement errors (impacting T and G) on the resulting IC:CG ratio, so this issue is not addressed here. For this work, we carried out a sensitivity analysis to explore the relative numerical stability of F_c and R as a function of the measured T and G density values (see appendix B for details). In summary, both F_c and R have low sensitivity to uncertainty in T for (typical) R values in the range of 1–10 (F_c between 0.5 and 0.1). However, the sensitivity of R to uncertainty in G is more than twice that of F_c at an R value of 1.0, and grows rapidly to 12 times larger at an R value of 10. For this reason, we recommend adoption of F_c (IC fraction) in future work.

In the work presented here, both the IC:CG ratio and IC fraction are plotted as a smoothed grid maps with the

“native” $0.5^\circ \times 0.5^\circ$ resolution, facilitating localized interpretation of the results. The IC:CG ratio is then plotted as a highly smoothed contour map for direct comparison with Fig. 2 in B01.

3. Results and discussion

a. LIS and OTD differences

A detailed comparison of the OTD and LIS flash densities is provided below, with the help of Fig. 1. LIS was limited to 37°N in this figure to discard the bias error near the edges due to smoothing. The flash densities range from 35 to 40 flashes $\text{km}^{-2} \text{ yr}^{-1}$ in Florida and western Mexico, to less than 1.0 along the U.S. West Coast and northeastern Canada. Both OTD and LIS (Figs. 1a and 1b, respectively) generally agree about the maxima over Florida, Cuba, and western Mexico, but there are some differences between the datasets over the rest of the domain. The LIS density off the coast of the Carolinas transitions from high values over land, decreasing to smaller values over the ocean, and enhancing again over the Gulf Stream. This is not well depicted in the OTD density map. The percent difference between the two sets is shown in Fig. 1d. Negative (orange/red) values represent a bias toward LIS, and positive (green/blue) values represent a bias toward OTD. White regions are either “no data” or indicate differences less than 10%. The values are generally between $\pm 40\%$ with the largest differences in parts of the Gulf of Mexico,

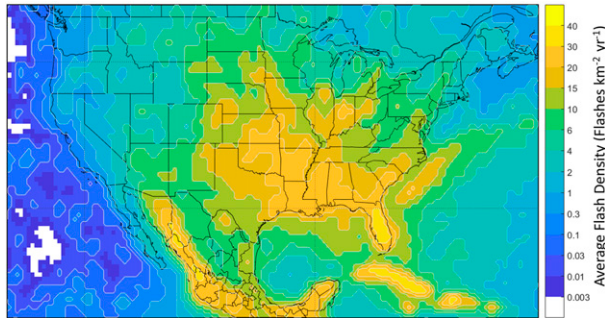


FIG. 2. The 18.5-yr climatology of the average flash density over CONUS from the combination of LIS and OTD data from HRFC. Contour lines are placed at all color boundaries above $0.01 \text{ flashes km}^{-2} \text{ yr}^{-1}$.

along the coast of the Gulf of California, and east and south of the Gulf Stream off the U.S. East Coast. For most of the United States (below 37°N) and over the water, visual inspection suggests that there may be some bias toward higher OTD density since there are more positive (blue) values. However, the average over the whole domain shows that the LIS reported 4% more lightning than OTD. If the differences were due to instrumental or calibration differences one would expect a more uniform bias toward either LIS or OTD. Additionally, the largest differences between the two datasets are spatially very close to each other, going from a negative extreme to a positive extreme. This finding is more likely associated with differences in the (orbital) sampling periods than with year-to-year variations in storm location since these two datasets have two years of overlap, although both factors are likely at work.

Given that the LIS density is a 15-yr climatology, it is reasonable to ascribe most of the variability to the OTD dataset. The sampling error analysis in appendix A provides quantitative support for this assertion. Specifically, the estimated fractional RMS error for individual grids in most of the LIS domain is between 0.03 and 0.10 (3%–10%). The “OTD only” region above 38°N exhibits larger relative RMS errors that are mostly in the range of 10% and 20%.

A histogram of the magnitude differences, accumulated from all the grid elements, is shown in Fig. 1c (bar graph), along with the associated cumulative distribution (line graph). About 50% of the grids have a variation of 20% or less, with monotonically decreasing likelihood of larger variations. Since many of these regional variations are larger than would be expected from the 10%–20% RMS random variations due to sampling for OTD, some of this variation must be due to interannual variability for the short OTD observation period. This is discussed further in the next section.

b. Multiyear variability using NLDN

As noted above, an underlying limitation of this analysis is the short (5 yr) observation period and limited view times for the combined satellite-derived climatology (see Fig. 2) above 38°N . Additional insight into this limitation is gained by comparing the NLDN climatologies over the same time periods (Fig. 3) following the analysis approach used for Fig. 1, since the NLDN provided continuous observations. The CG flash densities (corrected for detection efficiency) for the OTD and LIS periods are shown in Fig. 3a and 3b, respectively. The spatial distribution of lightning is strikingly similar during these two time periods, partly because of the common observations during 1998–2000. Differences are more readily observed in the percent difference map provided in Fig. 3d. Noteworthy contrasts include negative values (higher LIS density) during the late years throughout most of Texas, Kansas, Nebraska, and the northeastern United States, and positive values (higher OTD density) during the early years throughout much of the western states. Unlike the equivalent plot for OTD and LIS in Fig. 3d, the differences are more homogeneous over large areas, suggesting nonrandom variations over time that are likely due to natural decadal variations. A qualitative comparison of Figs. 1d and 3d shows little spatial coherence between the patterns in the two maps, suggesting that climatological factors are not dominating the spatial differences between the OTD and LIS datasets.

A histogram of the magnitude differences, accumulated for all grids, is shown in Fig. 3c (bar graph), along with the associated cumulative distribution (line graph). About 50% of the grids have a variation of 10% or less, with monotonically decreasing likelihood of larger variations. Since the NLDN density maps do not suffer from sampling limitations, all these differences are driven by interannual variability in storm occurrence. Comparing the frequency distributions in Figs. 1c and 3c, we infer that about half of the differences in the LIS and OTD densities are due to limited sampling for OTD and about half would then be due to interannual variability in the weather. Again, this is consistent with the expected sampling errors provided in appendix A.

The observations and interpretations provided above are what led us to derive the IC:CG ratio and IC fraction statistics using a modified NLDN CG flash density that was constructed to match the time periods of the satellite-derived climatologies (Fig. 4). This approach minimizes the short-term weather-related differences north of 38°N , but the sampling errors in the satellite-derived density remain.

c. Overall lightning climatology

The satellite and NLDN flash densities (Figs. 2 and 4, respectively) exhibit similar general patterns over CONUS.

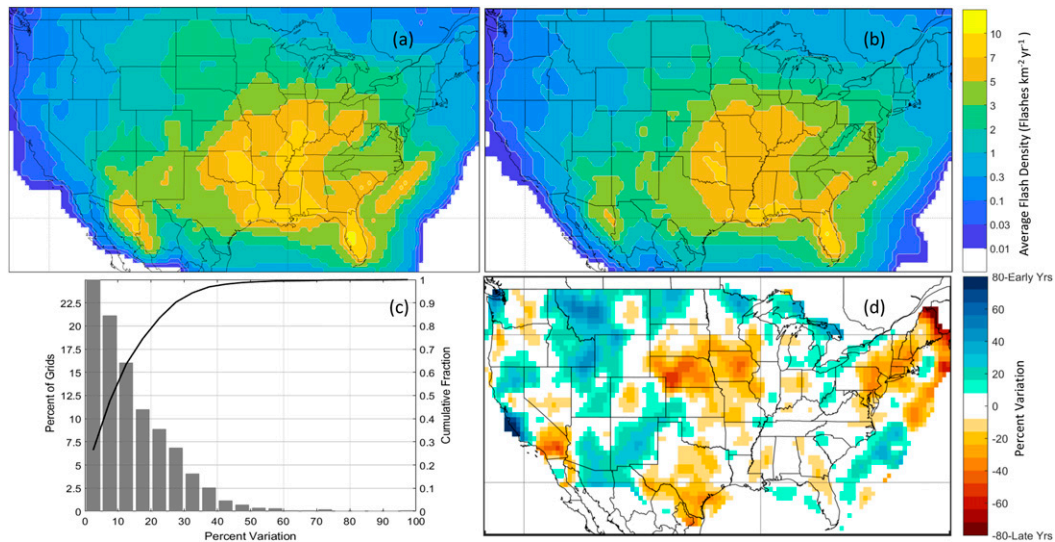


FIG. 3. Variability of NLDN ground flash density (GFD) for satellite observation periods: (a) NLDN GFD for the OTD observation period, (b) NLDN GFD for the LIS observation period, (c) spatial difference magnitude (% deviation from mean) histogram and cumulative distribution for NLDN GFD (OTD years – LIS years), and (d) spatial difference map for NLDN GFD (OTD years – LIS years). Negative values indicate higher density for LIS years. Contour lines in (a) and (b) are placed at all color boundaries.

The greatest CONUS flash densities are in Florida and the Gulf Coast, with a nearly steady fall-off to the west, northwest, and north. The 18.5-yr satellite climatology shows flash density maxima along the west coast of Mexico, as shown by [Murphy and Holle \(2005\)](#) and [Holle and Murphy \(2015\)](#). Other locally high density regions include the Gulf Stream and south-central United States. Furthermore, the Front Range of the Rocky Mountains has relatively higher density values (more lightning flashes) when compared to the central Rockies.

An important contributor for lightning along the Gulf Coast is deep low-level moisture driven from the very warm ocean waters ([Holle 2014](#)). When supplemented by coastal landmass heating, conditions are ideal for strong convection ([Stroupe et al. 2004](#)). The timing and modulation of lightning in this area is driven by several flow regimes, as described by [Smith et al. \(2005\)](#). There are also regions of high flash density over Florida. The driving factor for lightning here is the differential heating resulting from the thermal contrasts between land and ocean, helping to create convergent boundaries that trigger convection ([Hodanish et al. 1997](#); [Rudlosky and Fuelberg 2011](#)).

The well-defined lightning increase along the Gulf Stream off the East Coast is the result of locally warm waters that favor deep convection ([Christian et al. 2003](#)). More specifically, the increased lightning over this area compared to near-coastal waters has been associated with almost stationary convective clouds and precipitation associated with large fluxes of heat and water vapor from

the warm waters of the Gulf Stream to the colder air above ([Biswas and Hobbs 1990](#)). As with the Gulf Coast, lightning incidence in this area exhibits significant seasonal and diurnal modulation ([Virts et al. 2015](#); [Holle 2014](#); [Holle et al. 2016](#)). The low flash densities along/near the West Coast may result from the cold water and large-scale subsidence that inhibits deep convection, with local inland variations produced by the terrain-driven convection typically seen in the western United States ([Reap 1986](#)). A more in-depth discussion on the meteorological mechanisms for lightning in the United States can be found in [Lopez and Holle \(1986\)](#), [Holle et al. \(2016\)](#), and [Holle \(2014\)](#).

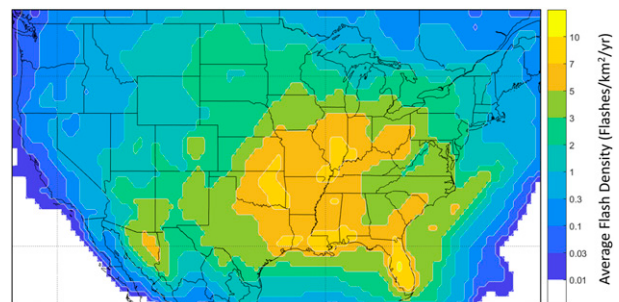


FIG. 4. GFD modified such that below 38°N the climatology includes May 1995–December 2013 (OTD + LIS observation period) and above 38°N the climatology only includes the OTD observation period. Contour lines are placed at all color boundaries.

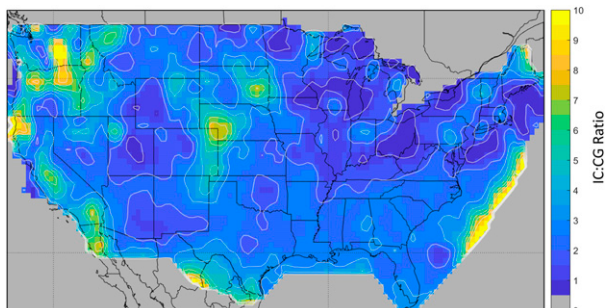


FIG. 5. The IC:CG ratio using LIS with NLDN for the 18.5-yr period and OTD with NLDN for the 5-yr period. Contour lines are placed at all color boundaries for ratios between 1.0 and 8.0, with steps of 1.0.

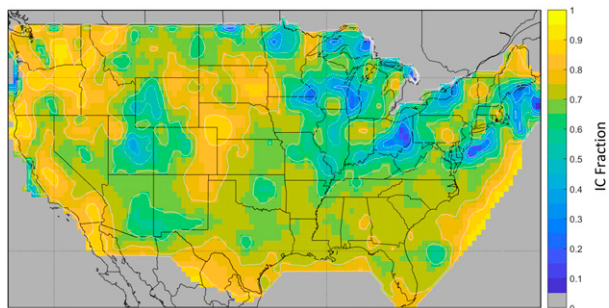


FIG. 6. The IC fraction using LIS with NLDN for the 18.5-yr period and OTD with NLDN for the 5-yr period. Contour lines are placed at all color boundaries for fractions between 0.35 and 0.85, with steps of 0.1.

d. IC:CG ratio and IC fraction

Equipped with an appreciation for the uncertainties in the satellite-derived TL flash density, the relative occurrence of IC and CG flashes can now be objectively explored. Figures 5 and 6 show the IC:CG ratio and IC fraction, respectively. There are no clear transitions from land to water in the Gulf of Mexico and the Atlantic coast, and there is no clear anomaly over the Gulf Stream. The high values at the southern and eastern extremes over the ocean and northern Mexico are due to the fall-off of NLDN DE with increasing distance from CONUS (not correctable). Most of the United States exhibits IC:CG ratio values between 1 and 4 (IC fraction between 0.5 and 0.8), with some notable exceptions. Distinctly high IC:CG ratio values occur in parts of eastern Colorado, Kansas, Nebraska, and South Dakota, clearly illustrated in both the IC fraction and IC:CG ratio. This region is well known from previous studies to be associated with high percentages of positive CG flashes when there is severe weather (Carey and Buffalo 2007; Carey and Rutledge 2003; Bruning et al. 2014).

Large IC:CG ratio values (>7) are also seen in the northwestern United States near Vancouver, Canada; portions of Washington and Oregon; and near the Northern California coast. B01 also reported high IC:CG ratio (Z) values in these areas, and suggested that this finding might not be significant due to the low flash density in the area. The error analysis carried out in appendix A provides a more quantitative assessment of this issue. It is shown (see Fig. A2) that the satellite RMS deviation is quite high in the coastal and western portions of Washington and Oregon, ranging from 35% to greater than 45% (darker blue regions). These larger uncertainties lead us to discount the extreme IC:CG ratio and IC fraction values found in western Washington, Oregon, and some regions near the Northern

California coast. This is not the case for southeastern Washington, western Idaho, and northeastern Oregon, or for central California, as discussed below.

Further noteworthy regions are identified in Fig. 7 and quantified in Table 2. Statistics associated with several parameters for these regions are derived from the grids that are within (or on) the dotted-line polygons shown in Fig. 7. The map in the top panel of Fig. 7 shows the IC fraction, and the map in the bottom panel shows the percentage of CG flashes that had a positive polarity

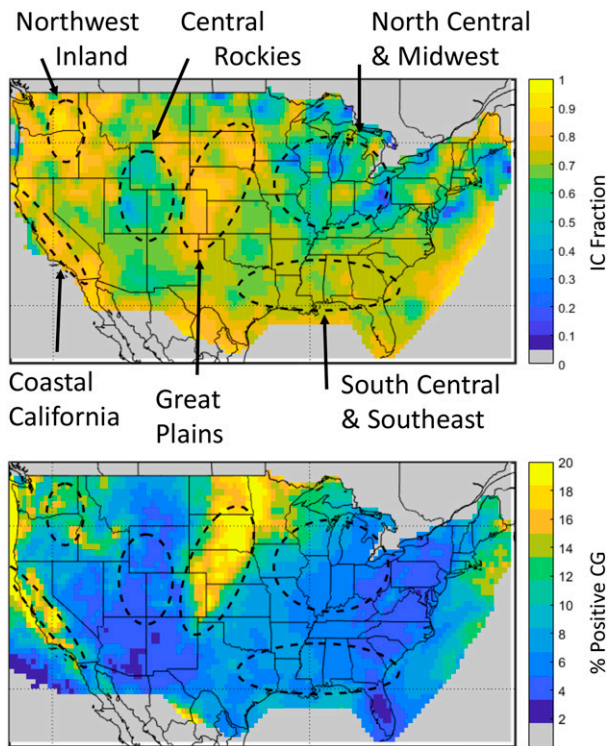


FIG. 7. Maps of (top) IC fraction and (bottom) percent positive CG flashes, identifying the six regions summarized in Table 2.

TABLE 2. Selected flash parameters [mean and standard deviation (SD)] for six regions shown in Fig. 7. The boldface rows indicate regions with very high IC fractions and the associated high percentages of positive CG flashes.

Region	Z (IC:CG) [Mean (SD)]	CG fraction [Mean (SD)]	IC fraction [Mean (SD)]	Percent positive CG [Mean (SD)]	Flash density [Mean (SD)]	Season	Time of day (local)
South-central	2.5 (0.25)	0.29 (0.02)	0.71 (0.02)	6.4 (0.87)	21.6 (3.5)	Summer	1400–1800
Coastal California	4.6 (1.7)	0.19 (0.05)	0.81 (0.05)	15.4 (3.8)	0.57 (0.39)	Spring + fall	0000–2400
Northwest inland	6.3 (2.4)	0.15 (0.06)	0.85 (0.06)	11.9 (1.5)	2.0 (0.80)	Summer	1800–0200
Great Plains	4.1 (1.3)	0.21 (0.05)	0.79 (0.05)	14.9 (3.7)	12.8 (2.8)	Summer	1800–0200
Central Rockies	1.6 (0.49)	0.40 (0.07)	0.60 (0.07)	5.3 (1.0)	4.2 (1.1)	Summer	1200–1600
North-central	1.5 (0.60)	0.44 (0.12)	0.56 (0.12)	7.0 (1.9)	11.6 (4.8)	Summer	1400–2200

(lowered positive charge to ground). Note the spatial coherence between these two parameters. The first three columns in Table 2 contain the mean and standard deviation (SD) for the three parameters reflecting the relative occurrence of IC and CG flashes, and the next two columns contain statistics for the percentage of positive flashes and the flash density, respectively. The last two columns indicate the dominant season and time of day for lightning in these regions, taken from work by Holle (2014) and Holle et al. (2016).

A south-central region is included in Table 2 because it represents a large region with homogeneous, “typical” IC:CG ratio (2.7) and IC fraction (0.73). This region has a high mean annual incidence of satellite-derived total lightning ($21.6 \text{ flashes km}^{-2} \text{ yr}^{-1}$, see also Fig. 4) that occurs during winter, spring, and summer, with most occurring in midsummer (July and August) between 14 and 18 h local time. This region also exhibits a typical percentage of positive CG flashes (6.4%).

The next three regions in the table (boldface rows) have very high IC fractions, and associated high percentages of positive CG flashes. Coastal California exhibits an average IC fraction of 0.81, with only 19% of the flashes including attachment to ground. A total of 15.4% of the reported CG flashes were positive, which is the largest percentage within the CONUS landmass. Although the statistical variability of any one grid in this region is suspect due to the low flash density ($<0.6 \text{ flashes km}^{-2} \text{ yr}^{-1}$), it is statistically impossible for this very large region to randomly exhibit such uniformly high IC fraction values. The storms in this region seem to occur in the spring or fall, randomly throughout the day, and likely differ from the more typical warm season thunderstorms that occur in the south-central region (low IC fraction) or in the Great Plains region discussed below (high IC fraction).

There is one small area in the northwest (northwest inland region in Table 2) where the exceptionally high IC:CG ratio (6.3) and IC fraction (0.85) values appear to be statistically reliable, even though the mean incidence of lightning is only $2 \text{ flashes km}^{-2} \text{ yr}^{-1}$. In appendix A

(see Fig. A2) it is indicated that the RMS uncertainty for the satellite-derived flash density in eastern Oregon, southwestern Idaho, and southeastern Washington (located west of the Blue Mountains in northeastern Oregon and southeastern Washington) is between 11% and 25%. This makes it possible to view the local high mean values in this area as meaningful, particularly when aggregated over the region. Portions of this area also exhibit high percentages of positive CG lightning (see Fig. 7), with an average value in the region of 11.9%. Storms in this area generally produce lightning in the summer months in the evening to nighttime hours.

The last region exhibiting a very high IC fraction (0.79) and IC:CG ratio (4.1) is a large portion of the central and northern Great Plains. Most of the lightning in this region occurs in the early evening to nighttime, and is most common during the summer. As noted earlier, this region also exhibits a large fraction of positive CG flashes (mean of 14.9%), the onset of CG flashes is frequently delayed relative to IC flashes (MacGorman et al. 2011), and it is a region where the percentage of positive CG flashes is substantially higher in severe storms (Carey and Rutledge 2003).

The last two rows in Table 2 are for two regions with low IC fractions. The central Rockies region exhibited a mean IC:CG ratio of 1.6 and an IC fraction of 0.6, with 40% of all flashes including CG strokes to ground. This large region sits geographically between the three regions with high IC fractions discussed earlier, and is within the highest and most-extensive mountain range within CONUS. The region also exhibits a distinctly low percentage of positive flashes (5.3%). Most of the lightning in this region occurs in the early to mid-afternoon (1200–1600, local time), well before storms occur in the Great Plains (Holle 2014, their Fig. 9a), and almost all thunderstorms occur during summer months. The north-central region exhibited the lowest mean IC:CG ratio (1.5) and an IC fraction (0.56), with 44% of all flashes including CG strokes to ground. This large region sits geographically bounded on the south by the northern Mississippi and Ohio Rivers. It also exhibits a

quite low percentage of positive flashes (7%). The lightning in this region occurs throughout the afternoon and early night, and almost all thunderstorms occur during summer.

All three regions with high IC fraction also exhibit a high percentage of positive CG flashes, irrespective of the storm season or diurnal pattern of incidence. Conversely, the two regions with quite low IC fraction exhibit much lower percentages of positive CG flashes, also with no consistent diurnal behavior. Comparison of the two panels in Fig. 7 indicates that this covariation of IC fraction and percentage of positive CG flashes holds throughout most of CONUS. This finding suggests that a variety of climate regimes exhibit this behavior that has previously been associated with inverted and/or complex charge structures, as discussed in section 1. We note that the eastern North Dakota, northern Minnesota, western Wisconsin, and Lake Superior seem to provide the exception to this generalization. This area exhibits a high percentage of positive CG flashes, as an extension of the behavior in the Great Plains region, but the IC fraction is lower and variable. Our review of the seasonal and diurnal CG climatologies in Holle et al. (2016) and Holle (2014) indicates that roughly 30% of the storms in this area occur during fall, and that the western Great Lakes have nocturnal lightning associated with derechos, unlike most of the central Great Plains.

A comparison of the B01 4-yr IC:CG ratio climatology (expressed as Z in that work) and two variants of the new 18.5-yr climatology is shown in Fig. 8. Figure 8c is the smoothed and contoured representation of the DE-corrected results shown in Fig. 5. To illustrate the impact of these corrections, the data used to produce Fig. 8b were not corrected. All three maps show a clear maximum over Kansas, Nebraska, and South Dakota, as well as maxima over Washington, Idaho, Oregon, and central California. The common behavior for all three maps in the northern United States is expected given that our climatology above 38°N is only 25% larger than the one used in B01 (5 vs 4 yr). Similar patterns are seen in all three maps over the eastern United States and over the central Rocky Mountains. However, there are significant differences over Texas, with lower IC:CG ratio values for both updated climatologies (Figs. 8b,c), resulting in values in Texas that now better match the southeastern United States. This change is driven by low TL flash density in this area during the LIS years (see Fig. 1d), coupled with a much higher CG flash density during these same years (see Fig. 3d). Both the DE-corrected and uncorrected results indicate the southern portion of the Intermountain West exhibits a IC:CG ratio that is more like that found in the east-central United States than in the Southeast. We ascribe these

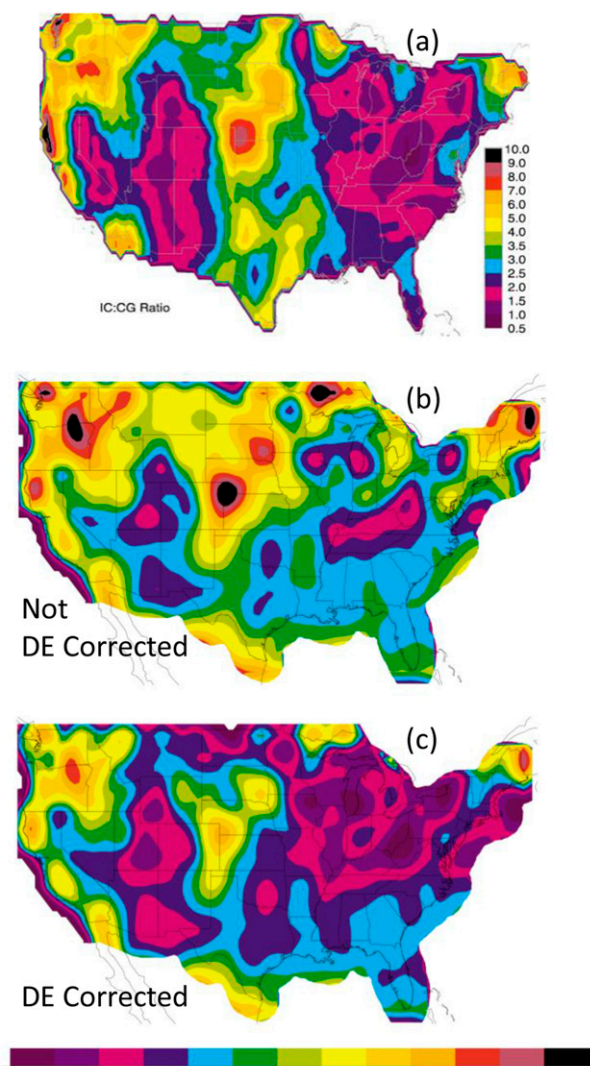


FIG. 8. IC:CG (Z) ratio comparison: (a) from B01, (b) IC:CG ratio from current study without correcting the NLDN detection efficiency, and (c) IC:CG ratio from current study using NLDN detection efficiency corrections described in appendix B. All datasets were smoothed and contoured in the same way.

differences from the original climatology produced by B01 to the much longer observation period south of 38°N, which does not suffer as much from both sampling errors and decadal-scale variations in weather patterns.

The accuracy of our estimates of the relative occurrence of IC and CG flashes deserves further discussion, beyond the uncertainty in IC:CG ratio that results from low and uncertain CG flash density (or counts). The area above 38°N may have additional uncertainty beyond that shown in appendix A (see Fig. A1) due to interannual variability and decadal variations in convective weather, but this was minimized by employing a time-matched CG flash dataset. Recently, concerns have

been raised about underestimation of satellite-derived flash density in northern Colorado where within-storm flash rates can be extremely high (Fuchs et al. 2016), and this issue could also apply to the central and upper Great Plains. This factor would only serve to increase the already significant positive anomaly in the IC:CG ratio and IC fraction in that area.

Moving on to the NLDN-derived CG flash incidence, its accuracy does not suffer from sampling issues, but several other factors contribute to its uncertainty. First, type classification (IC vs CG) by the NLDN is a known and characterized problem, with regional variations. Overall, the classification accuracy is expected to be about 90% (Nag et al. 2015; Zhu et al. 2016), but with poorer accuracy for low-current negative first strokes (<10 kA) in anomalously electrified storms that produce large percentages of CG flashes with positive polarity (Fleenor et al. 2009). We note that in our study the observation time period for most of the central Great Plains is limited to the OTD years (1995 to early 2000). During this period, only 2.5% of the negative first strokes reported by the NLDN had peak current magnitudes below 10 kA, due to poorer DE in those early years. If type classification in this region were a significant issue, the IC:CG ratio in Fig. 5 would likely show a discontinuity at 38°N near the Oklahoma–Texas border. As a second factor, the NLDN flash DE corrections described in the online supplemental material have uncertainties of about 10%, but likely vary up or down regionally around this value due to the type-classification errors noted above. The impact of this DE uncertainty is bounded by the differences between Figs. 8b and 8c (with and without corrections, respectively). The last factor impacting accuracy is the “definition of a flash,” first discussed in section 2c. Since we use flash density values produced separately by each system, any differences in the grouping of observations into flashes will clearly bias the results. If the 13% larger NLDN CG flash count found by Zhang et al. (2016) is accurate, and if it applies uniformly over our domain, then the observed IC fraction would be 17% too high for an IC fraction of 0.7, with higher (lower) percentages for higher (lower) IC fractions, respectively (in accordance with the sensitivities shown in Fig. B1).

4. Conclusions and future work

This study extends the IC:CG ratio climatology study carried out in B01 by employing larger datasets and including an analysis of IC fraction. We promote the use of the IC fraction parameter because of its greater statistical stability when small numbers of CG flashes are involved in the calculation. The strong correlation

between high IC:CG ratio and positive CG lightning in the central United States observed by B01 remains as a key and stable observation. Quantification of lightning characteristics in six selected large regions shows a consistent positive relationship between IC fraction and the percent of positive CG flashes, irrespective of lightning incidence (flash density), dominant season, and diurnal maximum period, thereby extending the correlation reported by B01 to large regions throughout CONUS. Our error analyses indicate that the high IC:CG ratio and IC fraction values observed in a small portion of northeastern Oregon and southeastern Washington, and in central California, likely reflect real climatological differences in these regions, and we have no clear explanations. The uncertainties in the observed dataset are not significant enough to discount these large and spatially coherent regional variations.

Several other observations extend and refine the findings by B01. The high IC:CG ratio (>4) throughout much of Texas reported by B01 is not reflected in this longer-term climatology, and this is likely the result of reduced sampling errors and more complete climatological observations. Both the NLDN and satellite datasets reported enhanced lightning over the Gulf Stream, but there was no clear variation in the relative occurrence of IC and CG flashes. There were also no abrupt changes at the Atlantic or Gulf of Mexico coastlines. This finding is interesting since estimated peak current (and energy) of first strokes in CG flashes is clearly enhanced offshore near the coastline (Orville et al. 2011; Cooray et al. 2014; Hutchins et al. 2013; Said et al. 2013; Nag and Cummins 2017).

The uncertainty in the satellite-derived lightning flash density climatology over CONUS was estimated using a statistical method and was shown to vary by region, providing a quantitative means to evaluate the significance of regional variations in lightning incidence and the relative occurrence of IC and CG flashes. Additionally, biases and variability in the satellite-derived lightning incidence due to nonuniform sampling by season and time of day are shown to be modest (a few percent).

Future efforts to assess weather and climate variations of the relative occurrence of IC and CG flashes using data from the Geostationary Lightning Mapper (GLM) should probably employ the GLM flash definition for all datasets. These flashes could then be assigned to be IC or CG depending either on the occurrence of CG strokes within the time–space domain of each flash, or on statistical classification of the IC fraction within the GLM dataset, as suggested by Koshak and Solakiewicz (2015). This will eliminate uncertainty due to differences in flash grouping.

Many important questions remain. The underlying mechanisms that modulate IC fraction are not fully understood, and the findings here suggest that they are not solely driven by flash rate (incidence) or storm intensity. There seems to be a positive correlation between IC fraction and the percentage of positive CG flashes in most regions, but the relationships are not unique. Terrain variations appear to help define boundaries between large regions with different IC fractions, but this is not always the case. A reliable global IC fraction climatology will likely add some clarity to the regional factors that modulate these relationships. Additionally, more consistent exploration of IC fraction and the percent of positive CG flashes in weather-related studies will help clarify mechanisms and may provide valuable information about the time evolution of severe weather.

Acknowledgments. We thank the NOAA GOES-R Program and the TRMM/LIS Science Team for the LIS/OTD data, for financial support, and for valuable input throughout this project. We are also grateful for the support under NASA Contract NNM12AA43C, and Program Announcement NNH14ZDA001N-INCA (Climate Indicators and Data Products for Future National Climate Assessments; Dr. Jack Kaye and Dr. Lucia Tsaoussi, NASA Headquarters). We also thank Vaisala for use of the NLDN data provided under contract. We individually thank Steve Goodman, Richard Blakeslee, and Dennis Buechler for encouragement and helpful discussions. Three anonymous reviewers and our AMS editor provided valuable input that greatly improved the manuscript. The OTD/LIS (1995–2013, <http://lightning.nsstc.nasa.gov>) and NLDN (1995–2013, <http://vaisala.com>) datasets are available. Spatial data for the NLDN yearly detection efficiency corrections, IC:CG ratio, and IC fraction are included in the supplemental material, in the form of geoTIFF files and Excel spreadsheets.

APPENDIX A

Satellite Sampling Errors

This appendix provides an analysis of errors in the satellite-derived lightning flash density resulting from limited view time. There are two sections: one that addresses random sampling errors due to limited total view time and one that addresses bias errors due to non-uniform sampling over both season and time of day.

a. Sampling errors

One of the most significant sources of error in the satellite-derived flash density is the limited view time for

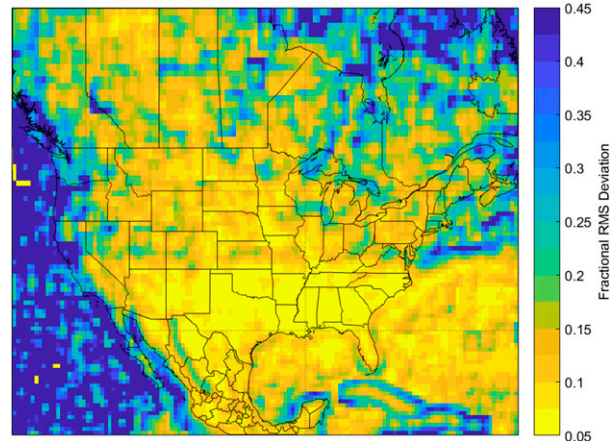


FIG. A1. Satellite fractional RMS deviation.

any given location on Earth. Over the contiguous United States, the yearly OTD view time is between 12 and 16 h, accumulated from numerous individual overpasses lasting about 3 min (Christian et al. 2003). The LIS annual view time over the contiguous United States is between 16 and 33 h, accumulated from numerous individual overpasses lasting about 90 s (C14).

An approximation to the RMS fractional error for each specific nonsmoothed $0.5^\circ \times 0.5^\circ$ grid can be produced by computing the standard deviation among that grid and its 24 nearest neighbors, and normalizing that value by an estimate of the mean for that grid location. The likely existence of some correlation among this grid value will tend to reduce the measured variation, and any underlying variation in the true lightning incidence will increase it. Since the nonsmoothed High Resolution Flash Climatology (HRFC) data were used in the initial error calculation, the resulting value must be scaled down by the expected error reduction resulting from applying a 5×5 grid Gaussian filter with a 1-grid standard deviation as was done to produce the flash density analyses in this paper (see the methods section in section 2). If one assumes that these 25 grids have independent measurement errors, then the smoothing will reduce the standard deviation by a multiplicative factor of 0.287 (based on the specific weights in the Gaussian filter).

This calculation, shown in Fig. A1, serves as an upper bound because it also includes true local variations that can occur within the roughly 140-km radius used for smoothing around a half-degree grid region. The dark blue areas near high-error (lighter blue) regions have RMS deviations greater than 0.45 times the mean, and the bright yellow areas have errors at or below 0.07 (7%) of the mean. Most of the LIS domain within the United States (below 38°N) has fractional deviations below 0.1. The values are larger in western Arizona and Southern

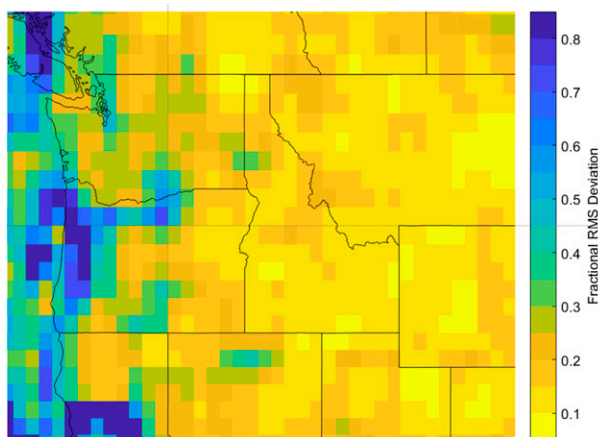


FIG. A2. Satellite fractional RMS deviation in the northwestern United States.

California due to lower flash density values. Most of the OTD domain in the United States exhibits RMS errors in the range of 0.1–0.25, except near the West Coast where flash densities are $<1 \text{ flash km}^{-2} \text{ yr}^{-1}$ (see Fig. 2 in the body of the paper). The large values (>0.25) off the coast of Florida, the Gulf of Mexico, the Gulf of California, and Cuba are due to the large gradient of flash density at the land–sea boundary (see Fig. 2), and therefore do not reflect actual sampling errors. Similarly, the large values off the northeast coast of the United States are collocated with a large spatial gradient of lightning density as the Gulf Stream swings eastward. Finally, the large values (dark blue) in northeast Canada are due to low flash density.

The uncertainty in the flash density in the northwestern United States is of great interest in this study, since there are portions of this area that exhibit IC fractions larger than those found in the central Great Plains (>0.9 ; see Fig. 6 in the body of the paper). Figure A2 provides a “zoom in” on the fractional deviation in this area. Although the color scale is limited to 0.85, there are values exceeding 1.5 (150%). The fractional deviation in northeast Oregon and southeast Washington are between 10% and 25%. This information is used in our interpretation of cloud fraction and Z ratio in the northwestern United States.

As noted above, there is concern that this analysis overestimates the RMS fractional error in regions where the actual spatial gradient of flash density is high. To address this concern, one of the authors (KLC) has undertaken an extensive statistical study of this sampling uncertainty that employs NLDN data. Results from this study provide very similar error estimates, and these will be published in a separate technical manuscript.

These estimates of random error due to limited view time do not address bias errors associated with non-uniform sampling as a function of season or time of day. This is addressed in the following section of this appendix.

b. View time biases

View time biases occurred for both diurnal and seasonal time references. The seasonal variation in sampling, which can be viewed as a monthly sampling problem, occurred because of extended periods of missing data. For OTD, there were 31 periods through the 5-yr mission with more than 2 consecutive days of missing data. For all months except for June, OTD produced data for 80%–93% of the available view time. OTD observed data for only 67% of the available view time for June. Moving on to the diurnal sampling variation, this occurred as a direct result of the satellite orbit, as well as missing data. For OTD, diurnal view time varied somewhat by region, but was about a factor of 2 within a region, having a sinusoidal pattern.

In this appendix, we evaluate these two view time biases through the United States and their potential impact on results provided in this paper. NASA’s HRFC and Low Resolution Full Climatology (LRFC) flash densities are not corrected for seasonal and diurnal view time biases. However, unbiased annual flash density climatologies can be formed from the diurnal and monthly climatologies provided in their High Resolution Monthly Climatology (HRMC) and Low Resolution Diurnal Climatology (LRDC) datasets, as discussed below (see C14 for further details).

For the monthly analysis, the HRFC and HRMC datasets were used. The values for each monthly HRMC map were scaled by the number of days in that month and then all monthly scaled values were added together to make an unbiased annual climatology. Since the “raw” HRMC data were already smoothed using a $2.5^\circ \times 2.5^\circ$ boxcar, the HRFC raw data were smoothed (prior to comparison) using the same boxcar filter. An “anomaly” dataset was produced by subtracting the HRFC climatology from the HRMC “monthly” climatology, then dividing by the average of the two, which was then expressed as a percentage. The results are shown in Fig. A3. A positive value indicates higher density for the monthly (unbiased) data while negative values indicate a higher density for the full climatology. There is very little difference in the LIS domain, and less than 10% difference in most of the OTD domain within the United States and north of about 38.5° latitude. Near 38°N there are large differences between the two datasets, which is a result of view-time-related differences between the LIS and OTD observations and the

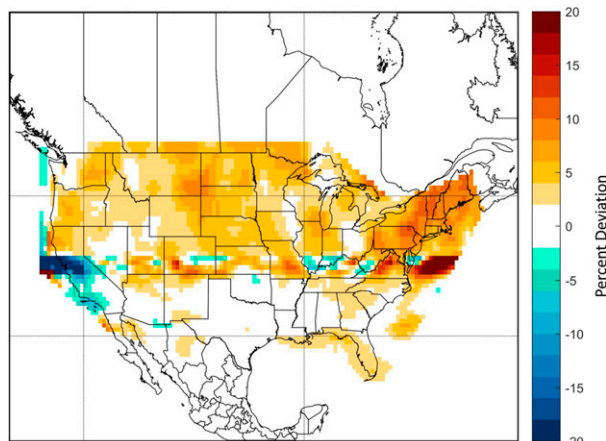


FIG. A3. The percentage difference between the HRMC monthly climatology and the HRFC boxcar filter climatology.

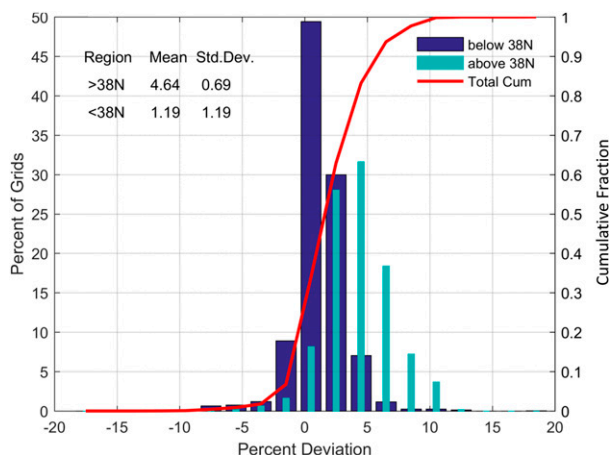


FIG. A4. Cumulative sum (line plot) and the histograms (bars) for the differences between the HRMC monthly climatology and the HRFC boxcar filter climatology.

associated smoothing. Figure A4 shows separate histograms of the percent deviation for north of 38°N and south of 38°N, as well as the cumulative distribution of the difference throughout CONUS. Data near 38°N were excluded from these histograms. This figure also includes the mean and standard deviations for the two regions. The mean difference above 38°N is +4.64%, indicating that the annual “full” (OTD) flash density may be somewhat low in that area. The associated percentage standard deviation is only 0.69%. The region below 38°N has a mean bias of 1.19%, with the same value for the standard deviation. Given the overall range of percent deviations between about -7% and +9% (see the red cumulative curve for all of CONUS), monthly sampling biases are not significant, particularly in the light of the underlying sampling errors shown in the first section of this appendix.

For the diurnal bias assessment, the LRDC and the LRFC datasets were used. The values for each hourly LRDC map were added together and scaled by 365.25 to create an unbiased annual climatology. Because of the large grids (2.5° × 2.5°) no additional smoothing was done. The low-resolution annual flash climatology was subtracted from this value for each grid, and their difference was divided by their mean and scaled to be a percentage. The results are presented in Fig. A5; here the positive values indicate higher density in the diurnal (unbiased) dataset while negative values indicate higher density for the full climatology. The areas with the largest (10%–20%) positive values are northern Nevada, Utah, western Colorado, and just east of New York.

Our area of interest in northeast Oregon, southeast Washington, and western Idaho exhibit a 5%–15% negative bias, suggesting that the uncorrected flash density is 5%–15% higher than one would get using the

diurnally normalized (unbiased) density. This is partially offset by the opposite-polarity bias in the monthly analysis described above, so we characterize the overall bias in this region as about 5%–10% too high in our satellite-derived flash density above 38°N. Our sensitivity analyses in appendix B suggest that a 10% overestimate of total lightning will result in a 1.2% overestimate of cloud fraction and a 10% overestimate of the IC:CG ratio in this area.

A similar set of histograms as those shown in Fig. A4 were generated for the diurnal percentage differences, and are shown in Fig. A6. The mean difference above 38°N is -2.21%. The associated standard deviation is only 2.81%, which is larger than the mean value. The region below 38°N has a mean bias of -0.12%, with an

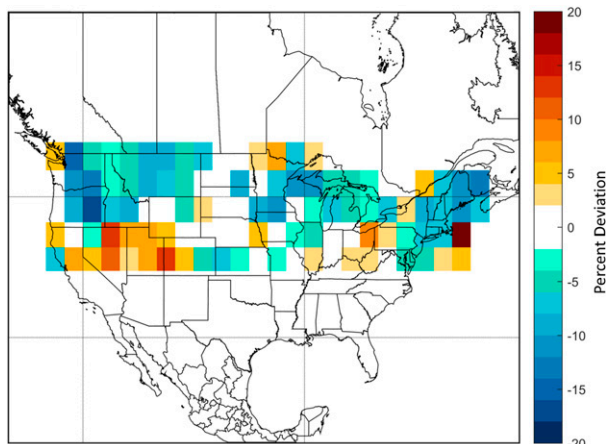


FIG. A5. The percentage difference between the LRDC diurnal climatology and the LRFC climatology.

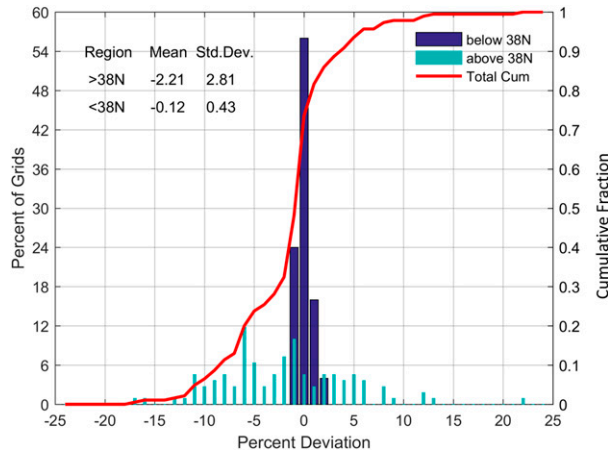


FIG. A6. Cumulative sum (line plot) and the histograms (bars) for the differences between the LRDC monthly climatology and the LRFC boxcar filter climatology.

associated standard deviation of 0.43%. The overall range of percent deviations is between about -16% and $+12\%$ (see the red cumulative curve for all of CONUS), established almost exclusively by errors in the OTD domain above 38°N . Although this error is not insignificant, it is still smaller than the typical sampling deviation in the northwestern United States, which is in the range of 20% – 30% (see Fig. A1). There is essentially no diurnal bias in the LIS domain below 38°N , because of the much longer observation period.

Given the modest monthly and diurnal biases, we have made the decision to employ the HRFC data for this study. If we corrected for these biases, the results would suffer by having to resort to low resolution ($2.5^\circ \times 2.5^\circ$) data. Nonetheless, local diurnal biases north of 38° are significant enough that they should be taken into consideration when interpreting the national-scale climatologies.

APPENDIX B

Sensitivity Analysis of IC:CG Ratio and IC Fraction

This appendix addresses the sensitivity of two ways of expressing the relative occurrence of IC and CG flashes to uncertainties in the measured quantities. We start with Eqs. (2) and (3) in the body of the paper that define the IC:CG ratio (defined as R for improved readability) and the IC fraction F_c , which is the fraction of lightning flashes that do not contact ground.

A sensitivity analysis was carried out to explore the numerical stability of F_c and R as a function of the measured T and G density values. This was accomplished by taking the total derivative of these functions as shown in the following equation:

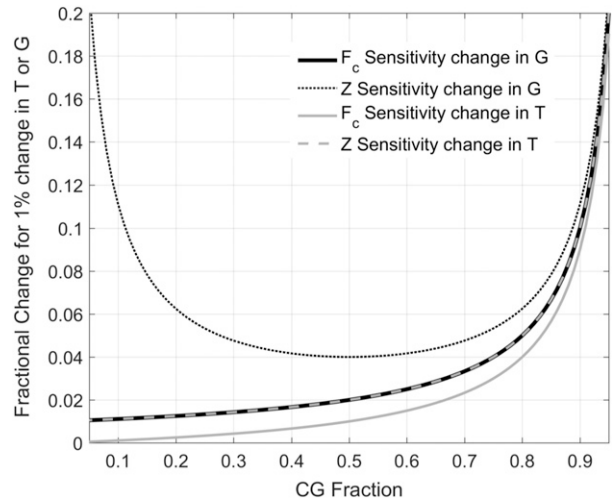


FIG. B1. Fractional sensitivity of IC:CG ratio Z and IC fraction F_c to a 1% change in total lightning T and CG fraction G , determined from the total derivative of these functions.

$$df(T, G) = \frac{\partial f}{\partial T} dT + \frac{\partial f}{\partial G} dG, \quad (\text{B1})$$

where f represents an arbitrary function with dependence on T and G . A convenient form for these sensitivity equations are shown below:

$$\frac{dF_c}{F_c} = \frac{1}{(T - G)} \left[\left(\frac{G}{T} \right) dT - dG \right] \quad (\text{B2})$$

$$\frac{dR}{R} = \frac{1}{(T - G)} \left[dT - \left(\frac{T}{G} \right) dG \right]. \quad (\text{B3})$$

It is evident that the sensitivities in Eqs. (B2) and (B3) share a common scale factor $(T - G)$, but important differences are seen in the second halves of the equations. In Eq. (B2), the G/T term “desensitizes” dT (since it is invariably less than 0.8; typically <0.5), while in Eq. (B3) the term T/G accentuates dG (since it is invariably greater than 1.2; typically >2.0).

Figure B1 shows the fractional sensitivity of the IC:CG ratio and IC fraction to a 1% change in G or the T counts, as a function of CG fraction. When there is a change of 1% in G ($dG = 0.01$) then dT is set to zero in the sensitivity equations, and vice versa for changes in T , to evaluate these effects separately. As the CG fraction gets small, the IC:CG ratio sensitivity to changes in G grows rapidly (dotted line), based on Eq. (B3). The IC fraction is far less sensitive to small changes in G (dark solid line). This analysis also shows that the IC fraction is minimally sensitive to changes in G and T for CG fractions in the range of 0–0.8, but it then becomes more sensitive at higher values. Since the climatological minimum IC:CG ratio found in B01 is 1.0 (IC fraction of

0.5), this sensitivity is not a practical problem. Also, note that neither IC:CG ratio nor IC fraction are highly sensitive to uncertainties in T density values.

REFERENCES

- Beirle, S., H. Huntrieser, and T. Wagner, 2010: Direct satellite observation of lightning-produced NO_x . *Atmos. Chem. Phys.*, **10**, 10 965–10 986, doi:10.5194/acp-10-10965-2010.
- , W. Koshak, R. Blakeslee, and T. Wagner, 2014: Global patterns of lightning properties derived by OTD and LIS. *Nat. Hazards Earth Syst. Sci.*, **14**, 2715–2726, doi:10.5194/nhess-14-2715-2014.
- Biswas, K. R., and P. V. Hobbs, 1990: Lightning over the Gulf Stream. *Geophys. Res. Lett.*, **17**, 941–943, doi:10.1029/GL017i007p00941.
- Boccippio, D. J., and Coauthors, 2000: The Optical Transient Detector (OTD): Instrument characteristics and cross-sensor validation. *J. Atmos. Oceanic Technol.*, **17**, 441–458, doi:10.1175/1520-0426(2000)017<0441:TOTDOI>2.0.CO;2.
- , K. L. Cummins, H. J. Christian, and S. J. Goodman, 2001: Combined satellite- and surface- based estimation of the intracloud-cloud-to-ground lightning ratio over the continental United States. *Mon. Wea. Rev.*, **129**, 108–122, doi:10.1175/1520-0493(2001)129<0108:CSASBE>2.0.CO;2.
- Bruning, E. C., and D. R. MacGorman, 2013: Theory and observations of controls on lightning flash size spectra. *J. Atmos. Sci.*, **70**, 4012–4029, doi:10.1175/JAS-D-12-0289.1.
- , S. A. Weiss, and K. M. Calhoun, 2014: Continuous variability in thunderstorm primary electrification and an evaluation of inverted-polarity terminology. *Atmos. Res.*, **135–136**, 274–284, doi:10.1016/j.atmosres.2012.10.009.
- Carey, L. D., and S. A. Rutledge, 1998: Electrical and multiparameter radar observations of a severe hailstorm. *J. Geophys. Res.*, **103**, 13 979–14 000, doi:10.1029/97JD02626.
- , and —, 2003: Characteristics of cloud-to-ground lightning in severe and nonsevere storms over the central United States from 1989–1998. *J. Geophys. Res.*, **108**, 4483, doi:10.1029/2002JD002951.
- , and K. M. Buffalo, 2007: Environmental control of cloud-to-ground lightning polarity in severe storms. *Mon. Wea. Rev.*, **135**, 1327–1353, doi:10.1175/MWR3361.1.
- Cecil, D. J., D. E. Buechler, and R. J. Blakeslee, 2014: Gridded lightning climatology from TRMM-LIS and OTD: Dataset description. *Atmos. Res.*, **135–136**, 404–414, doi:10.1016/j.atmosres.2012.06.028.
- , —, and —, 2015: TRMM LIS climatology of thunderstorm occurrence and conditional lightning flash rates. *J. Climate*, **28**, 6536–6547, doi:10.1175/JCLI-D-15-0124.1.
- Christian, H. J., and Coauthors, 2003: Global frequency and distribution of lightning as observed from space by the Optical Transient Detector. *J. Geophys. Res.*, **108**, 4005, doi:10.1029/2002JD002347.
- Cooray, V., R. Jayaratne, and K. L. Cummins, 2014: On the peak amplitude of lightning return strokes striking the sea. *Atmos. Res.*, **149**, 372–376, doi:10.1016/j.atmosres.2013.07.012.
- Cummins, K. L., and M. J. Murphy, 2009: An overview of lightning locating systems: History, techniques, and data uses, with an in-depth look at the U.S. NLDN. *IEEE Trans. Electromagn. Compat.*, **51**, 499–518, doi:10.1109/TEMC.2009.2023450.
- , —, E. A. Bardo, W. L. Hiscox, R. B. Pyle, and A. E. Pifer, 1998: A combined TOA/MDF technology upgrade of the U.S. National Lightning Detection Network. *J. Geophys. Res.*, **103**, 9035–9044, doi:10.1029/98JD00153.
- Driscoll, K. T., R. J. Blakeslee, and M. E. Baginski, 1992: A modeling study of the time-averaged electric currents in the vicinity of isolated thunderstorms. *J. Geophys. Res.*, **97**, 11 535–11 551, doi:10.1029/92JD00857.
- , —, and W. J. Koshak, 1994: Time-averaged current analysis of a thunderstorm using ground-based measurements. *J. Geophys. Res.*, **99**, 10 653–10 661, doi:10.1029/94JD00098.
- Fierro, A. O., A. J. Clark, E. R. Mansell, D. R. MacGorman, S. R. Dembek, and C. L. Ziegler, 2015: Impact of storm-scale lightning data assimilation on WRF-ARW precipitation forecasts during the 2013 warm season over the contiguous United States. *Mon. Wea. Rev.*, **143**, 757–778, doi:10.1175/MWR-D-14-00183.1.
- , J. Gao, C. L. Ziegler, K. M. Calhoun, E. R. Mansell, and D. R. MacGorman, 2016: Assimilation of flash extent data in the variational framework at convection-allowing scales: Proof-of-concept and evaluation for the short-term forecast of the 24 May 2011 tornado outbreak. *Mon. Wea. Rev.*, **144**, 4373–4395, doi:10.1175/MWR-D-16-0053.1.
- Fleener, S. A., C. J. Biagi, K. L. Cummins, E. P. Krider, and X. M. Shao, 2009: Characteristics of cloud-to-ground lightning in warm-season thunderstorms in the Great Plains. *Atmos. Res.*, **91**, 333–352, doi:10.1016/j.atmosres.2008.08.011.
- Franklin, V., 2013: An evaluation of the Lightning Imaging Sensor with new insights on the discrimination of lightning flash and stroke detectability. M.S. thesis, Department of Atmospheric Sciences, University of Alabama-Huntsville, 105 pp.
- Fuchs, B. R., and Coauthors, 2015: Environmental controls on storm intensity and charge structure in multiple regions of the continental United States. *J. Geophys. Res. Atmos.*, **120**, 6575–6596, doi:10.1002/2015JD023271.
- , E. C. Bruning, S. A. Rutledge, L. D. Carey, P. R. Krehbiel, and W. Rison, 2016: Climatological analyses of LMA data with an open-source lightning flash-clustering algorithm. *J. Geophys. Res. Atmos.*, **121**, 8625–8648, doi:10.1002/2015JD024663.
- Gatlin, P., and S. J. Goodman, 2010: A total lightning trending algorithm to identify severe thunderstorms. *J. Atmos. Oceanic Technol.*, **27**, 3–22, doi:10.1175/2009JTECHA1286.1.
- Goodman, S. J., and Coauthors, 2013: The GOES-R Geostationary Lightning Mapper (GLM). *Atmos. Res.*, **125–126**, 34–49, doi:10.1016/j.atmosres.2013.01.006.
- Hodanish, S., D. Sharp, W. Collins, C. Paxton, and R. E. Orville, 1997: A 10-yr monthly lightning climatology of Florida: 1986–95. *Wea. Forecasting*, **12**, 439–448, doi:10.1175/1520-0434(1997)012<0439:AYMLCO>2.0.CO;2.
- Holle, R. L., 2014: Diurnal variations of NLDN-reported cloud-to-ground lightning in the United States. *Mon. Wea. Rev.*, **142**, 1037–1052, doi:10.1175/MWR-D-13-00121.1.
- , and M. J. Murphy, 2015: Lightning in the North American monsoon: An exploratory climatology. *Mon. Wea. Rev.*, **143**, 1970–1977, doi:10.1175/MWR-D-14-00363.1.
- , K. L. Cummins, and W. A. Brooks, 2016: Seasonal, monthly, and weekly distributions of NLDN and GLD360 cloud-to-ground lightning. *Mon. Wea. Rev.*, **144**, 2855–2870, doi:10.1175/MWR-D-16-0051.1.
- Hutchins, M. L., R. H. Holzworth, K. S. Virts, J. M. Wallace, and S. Heckman, 2013: Radiated VLF energy differences of land and oceanic lightning. *Geophys. Res. Lett.*, **40**, 2390–2394, doi:10.1002/grl.50406.

- Jacobson, E. A., and E. P. Krider, 1976: Electrostatic field changes produced by Florida lightning. *J. Atmos. Sci.*, **33**, 103–117, doi:10.1175/1520-0469(1976)033<0103:EFPCBF>2.0.CO;2.
- Koshak, W., and R. J. Solakiewicz, 2015: A method for retrieving the ground flash fraction and flash type from satellite lightning mapper observations. *J. Atmos. Oceanic Technol.*, **32**, 79–96, doi:10.1175/JTECH-D-14-00085.1.
- , H. Peterson, A. Biazar, M. Khan, and L. Wang, 2014: The NASA Lightning Nitrogen Oxides Model (LNOM): Application to air quality modeling. *Atmos. Res.*, **135–136**, 363–369, doi:10.1016/j.atmosres.2012.12.015.
- , K. L. Cummins, D. E. Buechler, B. Vant-Hull, R. J. Blakeslee, E. R. Williams, and H. S. Peterson, 2015: Variability of CONUS lightning in 2003–12 and associated impacts. *J. Appl. Meteor. Climatol.*, **54**, 15–41, doi:10.1175/JAMC-D-14-0072.1.
- Krehbiel, P. R., 1986: The electrical structure of thunderstorms. *The Earth's Electrical Environment*, E. P. Krider et al., Eds., National Academy Press, 90–113.
- Krider, E. P., R. C. Noggle, and M. A. Uman, 1976: A gated wideband magnetic direction-finder for lightning return strokes. *J. Appl. Meteor.*, **15**, 301–306, doi:10.1175/1520-0450(1976)015<0301:AGWMDF>2.0.CO;2.
- Livingston, J. M., and E. P. Krider, 1978: Electric fields produced by Florida thunderstorms. *J. Geophys. Res.*, **83**, 385–401, doi:10.1029/JC083iC01p00385.
- Lopez, R. E., and R. L. Holle, 1986: Diurnal and spatial variability of lightning activity in northeastern Colorado and central Florida during the summer. *Mon. Wea. Rev.*, **114**, 1288–1312, doi:10.1175/1520-0493(1986)114<1288:DASVOL>2.0.CO;2.
- MacGorman, D. R., and W. D. Rust, 1998: *The Electrical Nature of Storms*. Oxford University Press, 432 pp.
- , D. W. Burgess, V. Mazur, W. D. Rust, W. L. Taylor, and B. C. Johnson, 1989: Lightning rates relative to tornadic storm evolution on 22 May 1981. *J. Atmos. Sci.*, **46**, 221–250, doi:10.1175/1520-0469(1989)046<0221:LRRTTS>2.0.CO;2.
- , I. R. Apostolopoulos, N. R. Lund, N. W. S. Demetriades, M. J. Murphy, and P. R. Krehbiel, 2011: The timing of cloud-to-ground lightning relative to total lightning activity. *Mon. Wea. Rev.*, **139**, 3871–3886, doi:10.1175/MWR-D-11-00047.1.
- Mach, D. M., H. J. Christian, R. J. Blakeslee, D. J. Boccippio, S. J. Goodman, and W. L. Boeck, 2007: Performance assessment of the Optical Transient Detector and Lightning Imaging Sensor. *J. Geophys. Res.*, **112**, D09210, doi:10.1029/2006JD007787.
- Mackerras, D., 1985: Automatic short-range measurement of the cloud flash to ground flash ratio in thunderstorms. *J. Geophys. Res.*, **90**, 6195–6201, doi:10.1029/JD090iD04p06195.
- , M. Darveniza, R. E. Orville, E. R. Williams, and S. J. Goodman, 1998: Global lightning: Total, cloud and ground flash estimates. *J. Geophys. Res.*, **103**, 19 791–19 809, doi:10.1029/98JD01461.
- Makowski, J. A., D. R. MacGorman, M. I. Biggerstaff, and W. H. Beasley, 2013: Total lightning characteristics relative to radar and satellite observations of Oklahoma mesoscale convective systems. *Mon. Wea. Rev.*, **141**, 1593–1611, doi:10.1175/MWR-D-11-00268.1.
- Mansell, E. R., C. L. Ziegler, and E. C. Bruning, 2010: Simulated electrification of a small thunderstorm with two-moment bulk microphysics. *J. Atmos. Sci.*, **67**, 171–194, doi:10.1175/2009JAS2965.1.
- Mareev, E. A., S. A. Yashunin, S. S. Davydenko, T. C. Marshall, M. Stolzenberg, and C. R. Maggio, 2008: On the role of transient current in the global electric circuit. *Geophys. Res. Lett.*, **35**, L15810, doi:10.1029/2008GL034554.
- Murphy, M. J., and R. L. Holle, 2005: Where is the real cloud-to-ground lightning maximum in North America? *Wea. Forecasting*, **20**, 125–133, doi:10.1175/WAF844.1.
- Nag, A., and V. A. Rakov, 2009: Some inferences on the role of lower positive charge region in facilitating different types of lightning. *Geophys. Res. Lett.*, **36**, L05815, doi:10.1029/2008GL036783.
- , and K. L. Cummins, 2017: Negative first stroke leader characteristics in cloud-to-ground lightning over land and ocean. *Geophys. Res. Lett.*, **44**, 1973–1980, doi:10.1002/2016GL072270.
- , M. J. Murphy, K. L. Cummins, A. E. Pifer, and J. A. Cramer, 2014: Recent evolution of the U.S. National Lightning Detection Network. *23rd Int. Lightning Detection Conf.*, Tucson, AZ, Vaisala, doi:10.13140/2.1.4443.1047, <http://www.vaisala.com/en/events/ildcilmc/Pages/ILDC-2014-archive.aspx>.
- , —, W. Schulz, and K. L. Cummins, 2015: Lightning locating systems: Insights on characteristics and validation techniques. *Earth Space Sci.*, **2**, 65–93, doi:10.1002/2014EA000051.
- Orville, E. R., G. R. Huffines, W. R. Burrows, and K. L. Cummins, 2011: The North American Lightning Detection Network (NALDN)—Analysis of flash data: 2001–09. *Mon. Wea. Rev.*, **139**, 1305–1322, doi:10.1175/2010MWR3452.1.
- Ott, L. E., and Coauthors, 2010: Production of lightning Nox and its vertical distribution calculated from three-dimensional cloud-scale chemical transport model simulations. *J. Geophys. Res.*, **115**, D04301, doi:10.1029/2009JD011880.
- Pinto, O., Jr., I. R. C. A. Pinto, and H. H. de Faria, 2003: A comparative analysis of lightning data from lightning networks and LIS sensor in the North and Southeast of Brazil. *Geophys. Res. Lett.*, **30**, 1073, doi:10.1029/2002GL016009.
- Qie, Z., T. Zhang, G. Zhang, T. Zhang, and X. Kong, 2009: Electrical characteristics of thunderstorms in different plateau regions of China. *Atmos. Res.*, **91**, 244–249, doi:10.1016/j.atmosres.2008.04.014.
- Reap, R. M., 1986: Evaluation of cloud-to-ground lightning data from the western United States for the 1983–84 summer seasons. *J. Climate Appl. Meteor.*, **25**, 785–799, doi:10.1175/1520-0450(1986)025<0785:EOCTGL>2.0.CO;2.
- Rudlosky, S. D., and H. E. Fuelberg, 2010: Pre- and postupgrade distributions of NLDN reported cloud-to-ground lightning characteristics in the contiguous United States. *Mon. Wea. Rev.*, **138**, 3623–3633, doi:10.1175/2010MWR3283.1.
- , and —, 2011: Seasonal, regional, and storm-scale variability of cloud-to-ground lightning characteristics in Florida. *Mon. Wea. Rev.*, **139**, 1826–1843, doi:10.1175/2010MWR3585.1.
- , and D. T. Shea, 2013: Evaluating WWLLN performance relative to TRMM/LIS. *Geophys. Res. Lett.*, **40**, 2344–2348, doi:10.1002/grl.50428.
- Said, R. K., M. B. Cohen, and U. S. Inan, 2013: Highly intense lightning over the oceans: Estimated peak currents from global GLD360 observations. *J. Geophys. Res. Atmos.*, **118**, 6905–6915, doi:10.1002/jgrd.50508.
- Schultz, C. J., W. A. Petersen, and L. D. Carey, 2011: Lightning and severe weather: A comparison between total and cloud-to-ground lightning trends. *Wea. Forecasting*, **26**, 744–755, doi:10.1175/WAF-D-10-05026.1.
- , L. D. Carey, E. V. Schultz, and R. J. Blakeslee, 2015: Insight into the kinematic and microphysical processes that control lightning jumps. *Wea. Forecasting*, **30**, 1591–1621, doi:10.1175/WAF-D-14-00147.1.
- Smith, J. R., H. E. Fuelberg, and A. I. Watson, 2005: Warm season lightning distributions over the northern Gulf of Mexico coast

- and their relation to synoptic-scale and mesoscale environments. *Wea. Forecasting*, **20**, 415–438, doi:10.1175/WAF870.1.
- Soriano, L. R., and F. de Pablo, 2007: Total flash density and the intracloud/cloud-to-ground lightning ratio over the Iberian Peninsula. *J. Geophys. Res.*, **112**, D13114, doi:10.1029/2006JD007624.
- Stauffer, R., G. J. Mayr, M. Dabernig, and A. Zeileis, 2015: Somewhere over the rainbow—How to make effective use of colors in meteorological visualizations. *Bull. Amer. Meteor. Soc.*, **96**, 203–215, doi:10.1175/BAMS-D-13-00155.1.
- Stroupe, J. R., H. E. Fuelberg, A. I. Watson, K. G. Kuyper, S. K. Rinard, and M. C. Koziara, 2004: Incorporating mesoscale lightning climatologies into the NWS IFPS/GFE forecast routine along the Gulf Coast. *20th Int. Conf. on Interactive Information and Processing Systems (IIPS) for Meteorology, Oceanography, and Hydrology*, Seattle, WA, Amer. Meteor. Soc., 8.12, https://ams.confex.com/ams/84Annual/techprogram/paper_70771.htm.
- Thompson, K. B., M. G. Bateman, and L. D. Carey, 2014: A comparison of two ground-based lightning detection networks against the satellite-based Lightning Imaging Sensor (LIS). *J. Atmos. Oceanic Technol.*, **31**, 2191–2205, doi:10.1175/JTECH-D-13-00186.1.
- Ushio, T., T. Wu, and S. Yoshida, 2015: Review of recent progress in lightning and thunderstorm detection techniques in Asia. *Atmos. Res.*, **154**, 89–102, doi:10.1016/j.atmosres.2014.10.001.
- Virts, K. S., J. M. Wallace, M. L. Hutchins, and R. H. Holzworth, 2015: Diurnal and seasonal lightning variability over the Gulf Stream and the Gulf of Mexico. *J. Atmos. Sci.*, **72**, 2657–2665, doi:10.1175/JAS-D-14-0233.1.
- Wiens, K. C., S. A. Rutledge, and S. A. Tessendorf, 2005: The 29 June 2000 supercell observed during STEPS. Part II: Lightning and charge structure. *J. Atmos. Sci.*, **62**, 4151–4177, doi:10.1175/JAS3615.1.
- Williams, E. R., 1989: The tripole structure of thunderstorms. *J. Geophys. Res.*, **94**, 13 151–13 167, doi:10.1029/JD094iD11p13151.
- , and Coauthors, 1999: The behavior of total lightning activity in severe Florida thunderstorms. *Atmos. Res.*, **51**, 245–265, doi:10.1016/S0169-8095(99)00011-3.
- Zhang, D., K. Cummins, A. Nag, and M. Murphy, 2016: Evaluation of the National Lightning Detection Network upgrade using the Lightning Imaging Sensor. *24th Int. Lightning Detection Conf. & Sixth Int. Lightning Meteor. Conf.*, San Diego, CA, Vaisala, <http://www.vaisala.com/en/events/ildcilmc/archive/Pages/ILDCILMC-2016-Archive.aspx>.
- Zhu, Y., V. A. Rakov, M. D. Tran, and A. Nag, 2016: A study of National Lightning Detection Network responses to natural lightning based on ground truth data acquired at LOG with emphasis on cloud discharge activity. *J. Geophys. Res. Atmos.*, **121**, 14 651–14 660, doi:10.1002/2016JD025574.